Journal of Glaciology

Supplementary Material for

Dynamic Models for Impact-Initiated Stress Waves through Snow Columns

S. V. Verplanck[1], E. E. Adams[1]

[1]Montana State University, Norm Asbjornson College of Engineering

Contents of this file

Text S1 to S4
Figures S1 to S10
Caption for Table S1
Tables S2 and S3

Additional Supporting Information (On Dryad Repository)

Tables S1 and S4
Figure generation scripts
Model implementation for finite difference and finite element methods
All considered regressions

Introduction

This document contains supporting information in the order in which they are referenced in the text. The separately uploaded files include model implementations and scripts used to generate the figures.

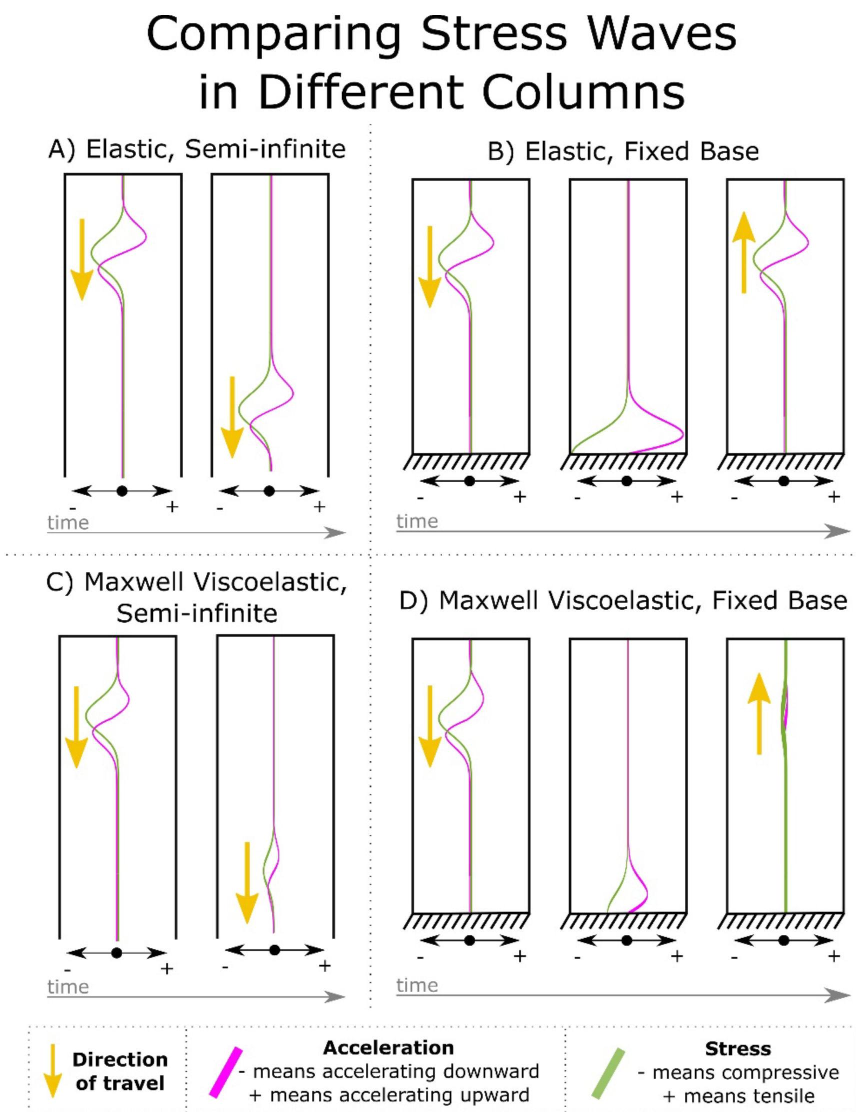

Fig. S1. Four configurations of elastic/viscoelastic rods which are semi-infinite/fixed at the base and subject to a compressive impact at the top of the rod. The double-sided arrow at the base of each column denotes the sign of stress and acceleration. Waves through both elastic and Maxwell-viscoelastic travel with a constant velocity. In the semi-infinite, elastic column (a) the stress wave travels downward never changing shape. In the elastic, fixed-bottom case (b), the positive interference between the incident and reflected compressive waves results in a peak compressive stress at the base which is double that of the applied stress. After interference has concluded, the original magnitude and shape is restored as an upwards traveling compressive wave. In the Maxwell, semi-infinite case (c), the wave decreases in magnitude as it travels through the column. Like the fixed-base elastic case, the fixed-base Maxwell case (d) results in positive interference between incident and reflected waves but the peak compressive stress is less than double the applied stress.

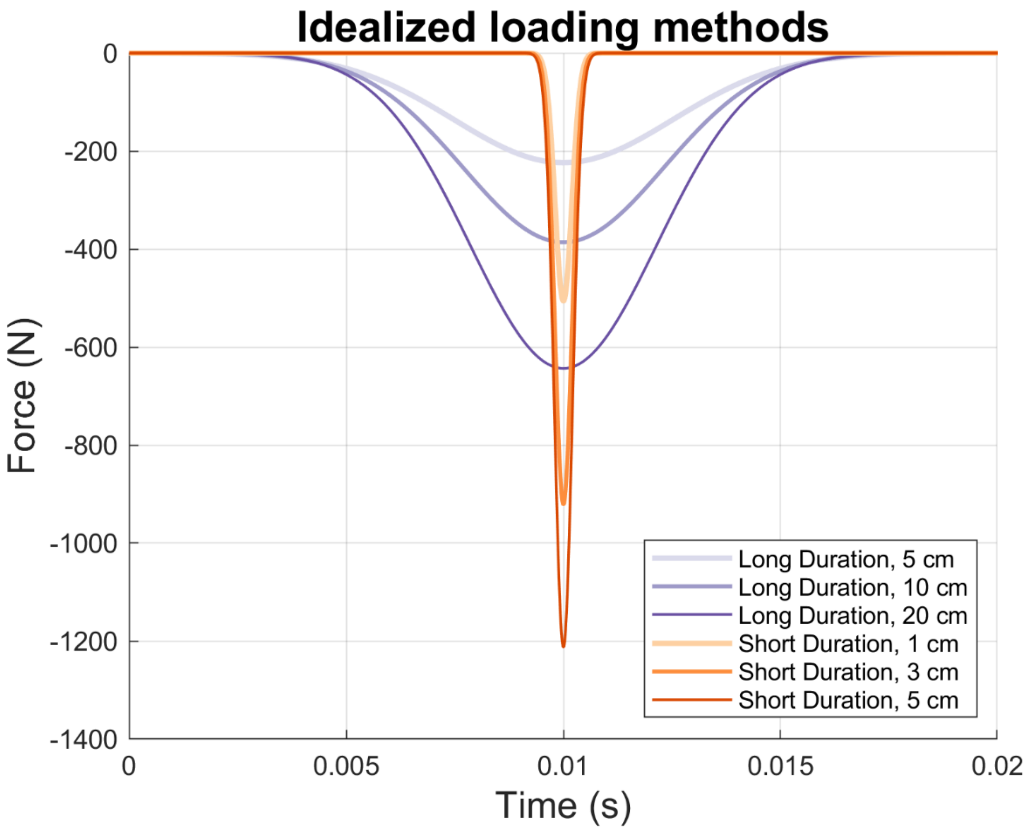

Fig. S2. A comparison of the six loading methods. The curves are idealized as Gaussians according to equation 8. The drops heights are shown in the legend and impact duration category are shown in the legend.

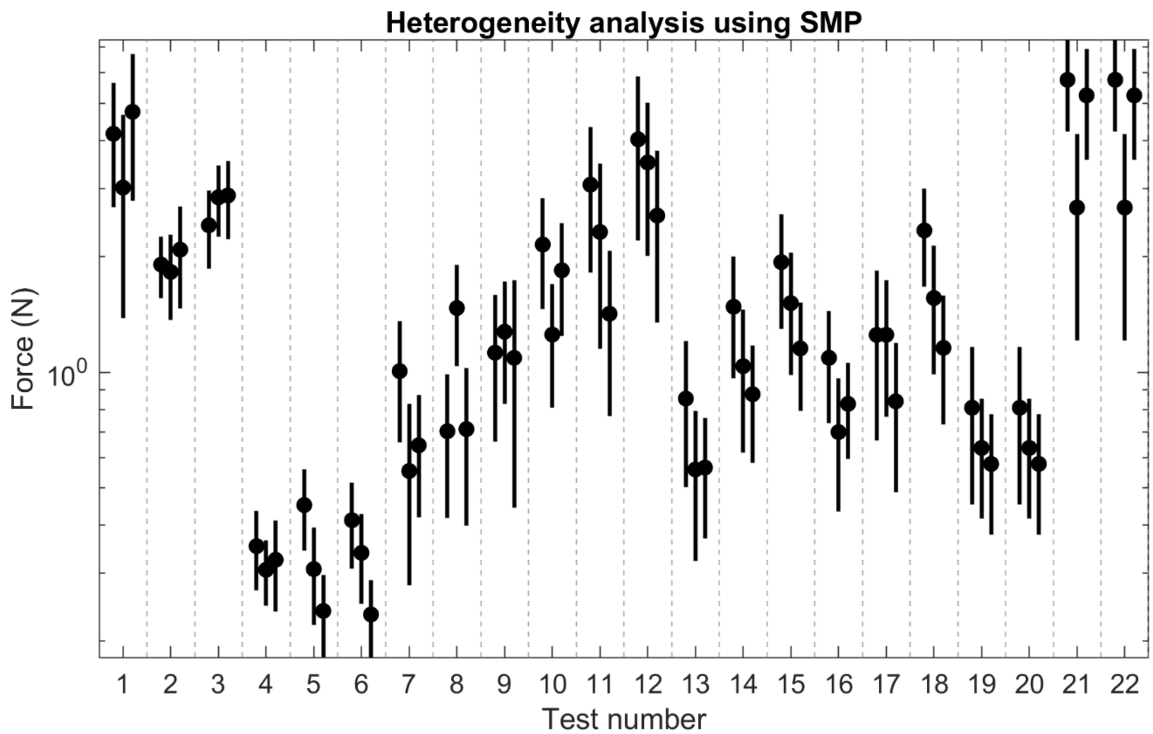

Fig. S3. An evaluation of the heterogeneity in the test samples. Each dot is the median force from the profile and the lines are one standard deviation in each direction. Three SMP measurements are made in each column to investigate horizontal heterogeneity, and the standard deviations for each profile are a measure of vertical heterogeneity. Tests 19/20 and 21/22 are identical because they use the same column for both short and long duration impacts. In 15 out of the 20 snow columns, all three error bars overlap indicating minimal horizontal heterogeneity. In the 5 remaining columns (tests 5,6,8,18, and 21/22), there is overlap by two out of the three error bars indicating a greater degree of horizontal heterogeneity. Keeping in mind the logarithmic scale, the degree of vertical heterogeneity tends to increase with penetration resistance. The SMP values used for the regression are the means of the three medians.

Table S1. Details on the snow columns that were tested including impact category, snow properties, and height change. The height change was measured with both a stick ruler and a SnowMicropen mounted to a stand at a fixed height. The table is uploaded to the Dryad repository with the filename: TableS1_detailedSnowTests.xlsx.

Text S1.

Since there is a significant (> 5 mm) change in height between impacts for the tests that took place on 9–11 November 2022, the height for each drop is calculated. This section describes the details of that process.

The height, H, is a function of the drop number, d, the applied impact forces, and the starting height of the column, H_s.

$$H(d) = \begin{cases} H_s - dm_{low} & 0 \le d \le 10 \\ H_s - 10m_{low} - (d-10)m_{mid} & 11 \le d \le 20 \\ H_s - 10m_{low} - 10m_{mid} - (d-20)m_{high} & 21 \le d \le 30 \\ H_s - 10m_{low} - 10m_{mid} - 10m_{high} - (d-30)m_{mid} & 31 \le d \le 40 \\ H_s - 10m_{low} - 10m_{mid} - 10m_{high} - 10m_{mid} - (d-40)m_{low} & 41 \le d \le 50 \end{cases} \quad \text{(S1)}$$

The slopes, m_{low},m_{mid}, and m_{high}, are different depending on their respective impact force. The slopes are calculated as ratios of the average peak forces for the three drop heights (see Table 1). The average peak force for the highest drop, F_{high}, is 2.9 times that of the average drop from the lowest height, F_{low}.

$$F_{high} = \alpha F_{low} \quad \text{(S2)}$$

Where $\alpha = 2.9$. Similarly, for the average peak force of the middle height, F_{mid}

$$F_{high} = \beta F_{mid} \quad \text{(S3)}$$

Where $\beta = 1.7$.

To calculate the slopes, the total change in height after 50 drops, ΔH, is used in concert with these ratios.

$$m_{low} = \frac{\Delta H}{20 + 20\frac{\alpha}{\beta} + 10\alpha} \quad \text{(S4)}$$

$$m_{mid} = \frac{\Delta H}{20\frac{\beta}{\alpha} + 20 + 10\beta} \quad \text{(S5)}$$

$$m_{high} = \frac{\Delta H}{\frac{20}{\alpha} + \frac{20}{\beta} + 10} \quad \text{(S6)}$$

For example, Fig. S3 illustrates the height changes over 50 drops on 9 November 2022.

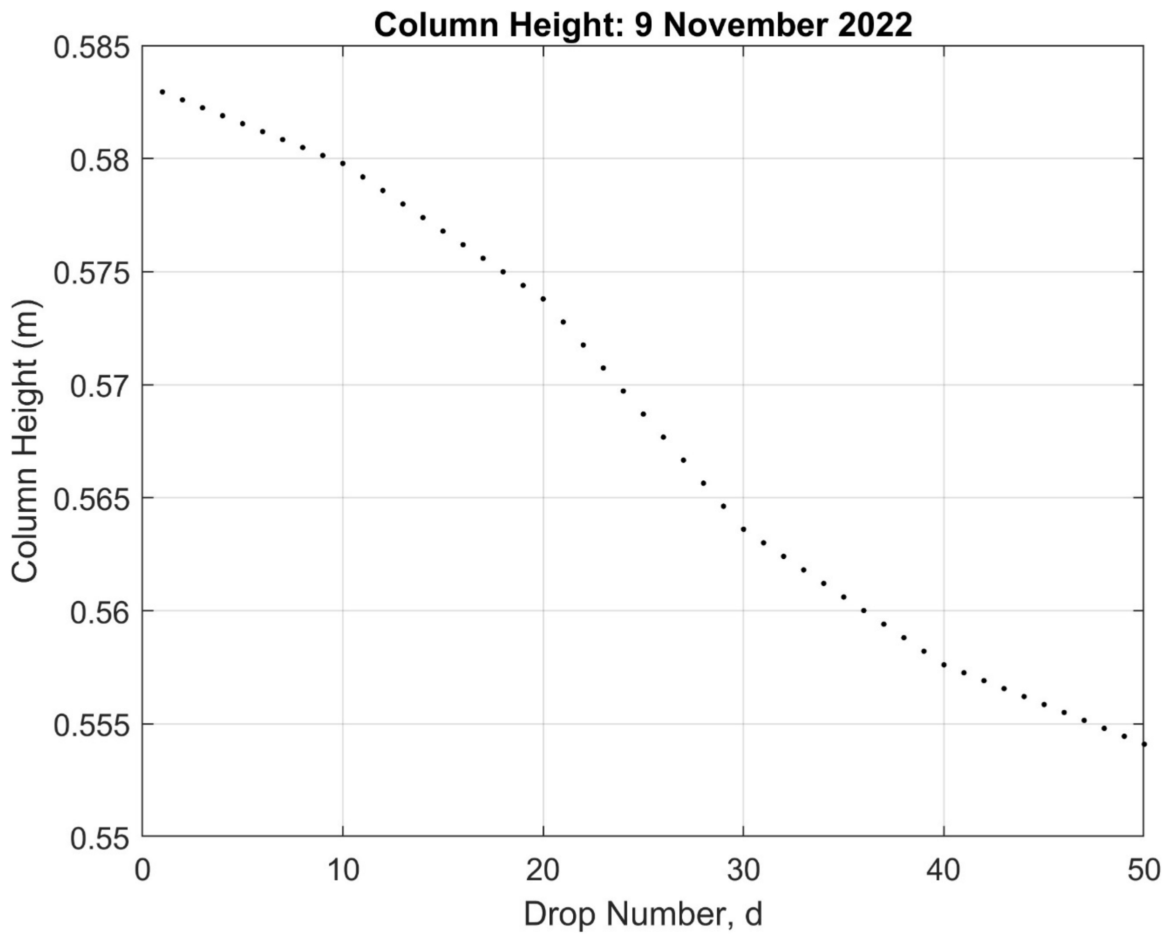

Fig. S4. The height is calculated for each individual drop based on a piecewise linear interpolation between the measured starting height and ending height on the test days where the height change was greater than 5 mm (9-11 November 2022).

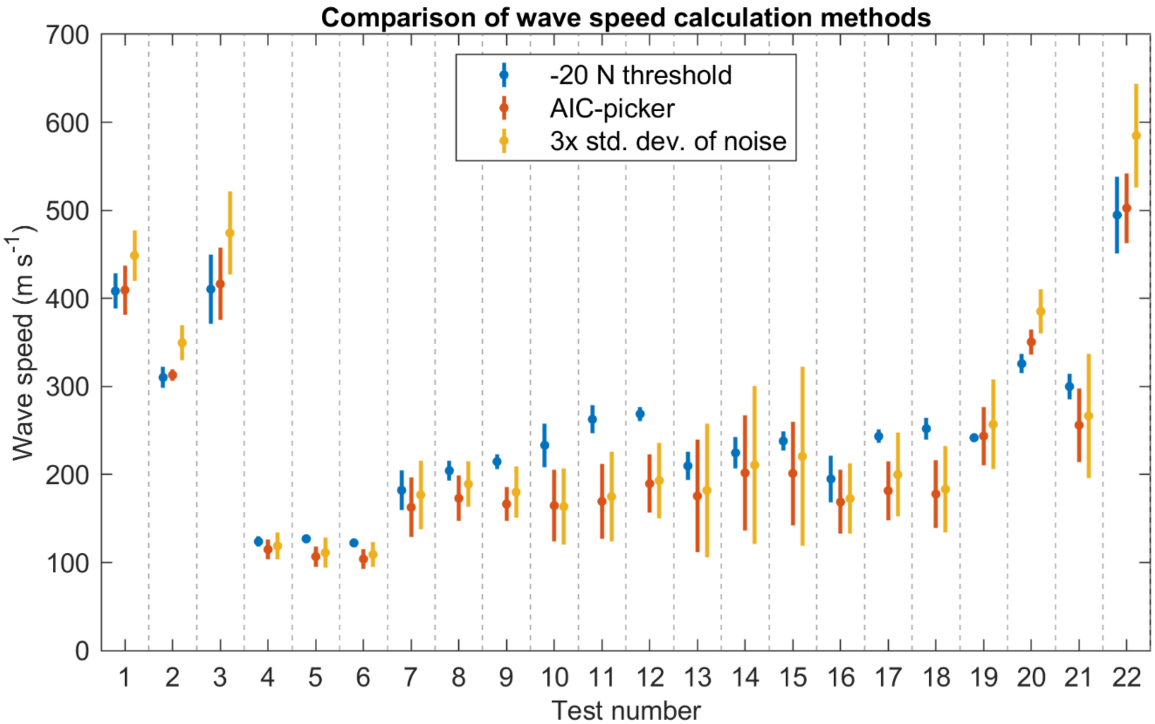

Fig. S5. To determine the arrival of the stress wave at each plate, three methods are considered. First, a fixed threshold -20 N. Second, an autoregressive approach, referred to as AIC-picker, that determines the minimum AIC of the continuous wavelet transform as the signal arrival time (Kurz and others 2005, Kalkan 2016). Third, a variable threshold equal to three times the standard deviation of the noise prior to the signal. These three methods are applied to the entire dataset. For the short duration impacts (tests: 1,2,3,20,22) the wave speed for the -20 N threshold and AIC-picker are of similar magnitude whereas the variable threshold based on the noise is of higher magnitude. For the long duration impacts (all other test numbers), the fixed, -20 N threshold appears to be systematically greater than the other two methods, which achieve similar results. Ultimately, the AIC-picker method is chosen for further analysis. The fact that the stress wave has attenuated as it transmits through snow opposes the use of a fixed value threshold. The greater variance in the noise-based threshold supports the use of the AIC-picker. Furthermore, this method was used in a similar study to measure the elastic modulus of snow with acoustic emissions sensors (Gerling and others, 2017).

Text S2. Example of regression determination

The process for selecting a regression model is exemplified for the elastic modulus, long duration impacts (E_{long}). The 7 possibilities of equation (S1) are calculated with density, ρ, thin blade penetration resistance, R_{TB}, and/or temperature, T. They are shown in Table S2.

$$\mathrm{E_{long}}(\rho, R_{TB}, \mathrm{T}) \approx \mathrm{a_0} + \mathrm{a_1}\rho + \mathrm{a_2}R_{TB} + \mathrm{a_3}\mathrm{T} \tag{S7}$$

Table S2. Seven regressions considered for $\boldsymbol{E_{long}}$, excluding interactions. The lowest $\boldsymbol{AIC_c}$ score is highlighted. The $\boldsymbol{R^2}$ and adjusted $\boldsymbol{R^2}$ ($\boldsymbol{R^2_{adj}}$) are included for reference but are not the criteria used for model selection.

Predictors	a_0 [Pa]	a_1 [m² s⁻²]	a_2 [m⁻²]	a_3 [Pa °C⁻¹]	R^2	R^2_{adj}	AIC_c
ρ	-8.45E+06	7.07E+04	0	0	0.70	0.68	559.3
R_{TB}	2.87E+06	0	1.01E+06	0	0.77	0.76	554.6
T	3.96E+06	0	0	-4.57E+05	0.13	0.07	577.6
ρ, R_{TB}	-2.61E+06	3.06E+04	6.72E+05	0	0.82	0.79	553.8
ρ, T	-1.12E+07	6.80E+04	0	-3.26E+05	0.76	0.73	558.3
R_{TB}, T	2.49E+06	0	9.94E+05	-4.37E+04	0.77	0.74	557.5
ρ, R_{TB}, T	-4.85E+06	3.56E+04	5.66E+05	-1.53E+05	0.83	0.79	556.2

The regression with lowest AIC_c score is the current front-runner which happens to include density and penetration resistance as predictors. Now there are interactions between the predictors to consider. Interactions were not considered earlier as to not violate the marginality principle (Weisberg, 2014). So, one more possible regression is considered.

$$\mathrm{E_{long}}(\rho, \mathrm{h_{SMP}}, \mathrm{T}) \approx \mathrm{a_0} + \mathrm{a_1}\rho + \mathrm{a_2}R_{TB} + \mathrm{a_4}\rho R_{TB} \tag{S8}$$

Table S3. The $\mathbf{E_{long}}$ regression with interactions between predictors considered.

Predictors	a_0 [Pa]	a_1 [m² s⁻²]	a_2 [m⁻²]	a_3 [Pa °C⁻¹]	a_4 [m² s⁻² N⁻¹]	R^2	R^2_{adj}	AIC_c
$\rho, R_{TB}, \rho R_{TB}$	-2.42E+06	3.21E+04	3.55E+05	0	7.75E+02	0.82	0.78	557.3

The regression that includes interactions has higher AIC_c values than the regression without interaction terms. Thus, the front-runner regression remains the one highlighted in Table S2.

The final consideration is using SMP penetration resistance instead of thin blade penetration resistance. It turns out, all of the regressions with SMP penetration resistance have higher AIC_c values than 553.8. Thus, the highlighted equation in Table S2 remains the recommended regression. The data for all regressions is included in the Dryad repository in the “Regressions” folder.

Text S3. Multicollinearity analysis

Multicollinearity may be a concern among the three predictor variables: density (ρ), penetration resistance (R_{SMP} or R_{TB}), and temperature (T). The correlation coefficient is a "measure of linear association" (Kutner et al., 2005) between two variables and spans from -1 to 1. The closer the absolute value of the coefficient is to 1, the more the variables are correlated; a value of 0 implies no correlation. As a step towards determining the degree of multicollinearity, correlation coefficient matrices are calculated for the four sets of predictors and are shown in Fig. S6.

a Long Duration, SMP

	ρ	R_{SMP}	T
ρ	1	0.83	-0.13
R_{SMP}	0.83	1	-0.40
T	-0.13	-0.40	1

b Long Duration, Thin Blade

	ρ	R_{TB}	T
ρ	1	0.81	-0.13
R_{TB}	0.81	1	-0.37
T	-0.13	-0.37	1

c Short Duration, SMP

	ρ	h_{smp}	T
ρ	1	0.91	0.42
R_{SMP}	0.91	1	0.09
T	0.42	0.09	1

d Short Duration, Thin Blade

	ρ	R_{TB}	T
ρ	1	0.92	0.42
R_{TB}	0.92	1	0.15
T	0.42	0.15	1

Fig. S6. The correlation coefficient matrices for the four sets of predictors

These matrices are of limited use because they only show the correlation between two variables, but one variable may be correlated to a linear combination of the two other variables. Thus, a common metric to determine the severity of multicollinearity is the variance inflation factor (VIF). VIF's are the diagonal terms of the inverse of the correlation coefficient matrix (Belsley et al., 1980). The VIF's for the four sets of predictors are shown in Fig. S7.

a Long Duration, SMP

	VIF
ρ	3.9
R_{SMP}	4.6
T	1.4

b Long Duration, Thin Blade

	VIF
ρ	3.2
R_{TB}	3.7
T	1.3

c Short Duration, SMP

	VIF
ρ	16.0
R_{SMP}	13.3
T	2.8

d Short Duration, Thin Blade

	VIF
ρ	14.1
R_{TB}	11.9
T	2.2

Fig. S7. The variance inflation factors (VIF's) for the four sets of predictors.

A predictor's VIF of 1 implies there is no correlation between that predictor and any linear combination of the other two predictors. When the VIF is higher, it indicates a stronger correlation and increases concern of multicollinearity. A commonly used threshold is 10 (Kutner et al., 2005). By that threshold, multicollinearity is a concern for the short impact duration tests' sets of densities and hardness (Fig. S6 parts c and d). So, any regression for these short impact duration tests that contains both density and hardness may be unreliable.

The low VIF for the long impact duration tests is attributed to the experimental design. Specifically, the densities remained constant for the three days of testing while the penetration resistance and temperature changed.

Text S4

There is inherent uncertainty in the determination model parameters. First, wave speed is calculated using column height and travel time. The uncertainty in column height is primarily driven by the levelness of the column, estimated to be ±4% (±2.5 mm with a 60 cm column). Uncertainty in travel time has both statistical and systematic components. The statistical component is the statistical spread across repeated loading events and is considered as the standard deviation of the AIC-picker method in **Fig. S5**. The systematic component is the uncertainty in determining travel time from the onset determination method (AIC-picker). Comparing the AIC-picker method to the other considered methods, the systematic uncertainty, as plotted in **Fig. S8**, is defined as the maximum percent difference in mean travel time between AIC-picker and the other two methods. In 21 of the 22 tests, this systematic uncertainty was larger than statistical uncertainty by these definitions. Sampling rate also contributes to systematic uncertainty an additional 1-2%, but is left off **Fig. S8** because of its relatively minor contribution.

The uncertainty in wave speed carries over to an uncertainty in elastic modulus, with the inclusion of density. The uncertainty in density is due to the scale resolution of ±1-4% (±0.5 g uncertainty, 13.5 g to 42.8 g samples) and volume uncertainty of ±2% (100 ± 2 cm^3). Following the elastic modulus is viscosity, which has the propagated uncertainty from elastic modulus in addition to an uncertainty associated with peak measured force at the column's base and stopping criteria in the root finding. This uncertainty in force is <1% (1 N/maximum measured peak force at base).

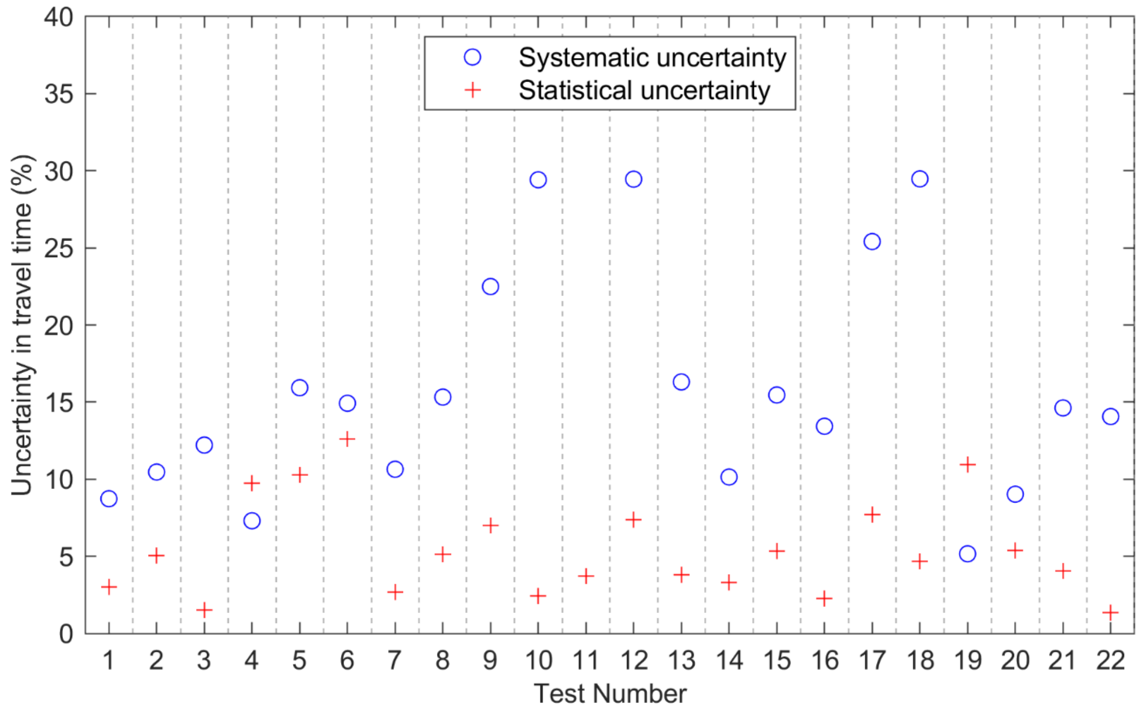

Fig. S8. A comparison of systematic and statistical uncertainty for travel time. The statistical uncertainty is the standard deviation of the ascertained travel times for each test number. The systematic uncertainty is the maximum percent difference in mean travel time between AIC-picker and the other two onset determination methods.

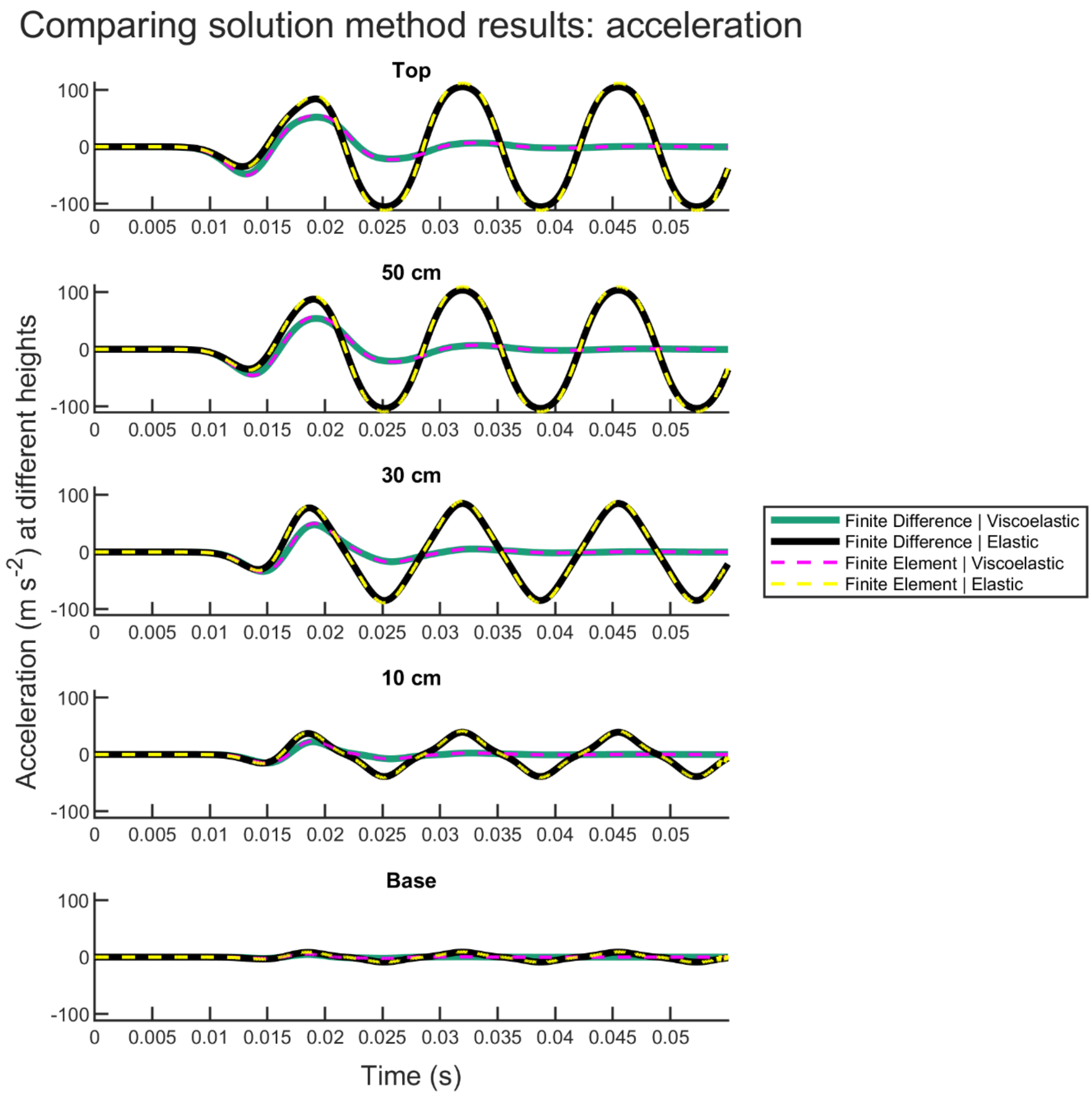

Fig. S9. A visual comparison of the acceleration results from the two different numerical solution methods of the governing equations. The results between the finite difference and finite element methods agree well with each other.

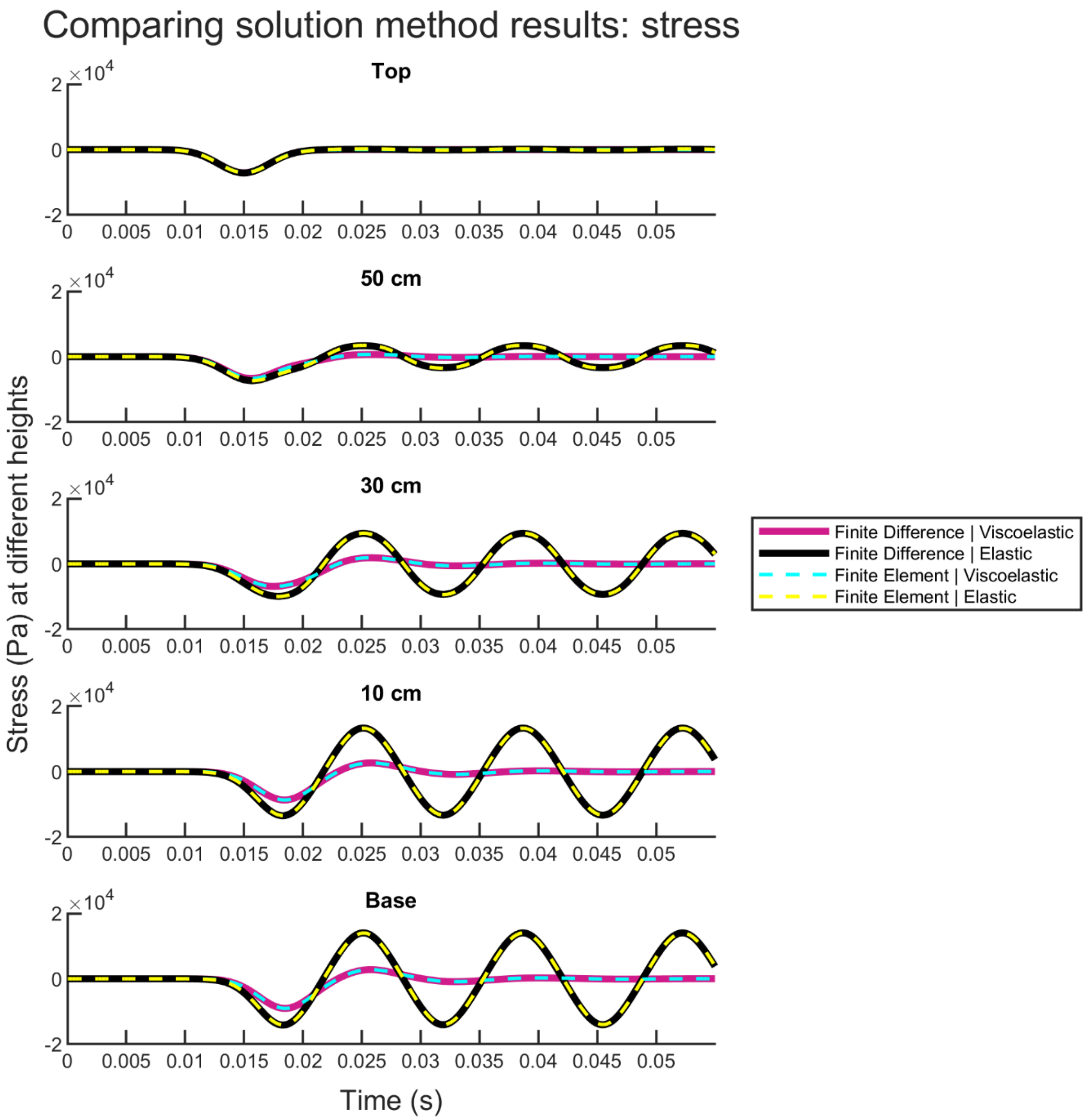

Fig. S10. A visual comparison of the stress results from the two different numerical solution methods of the governing equations. The results between the finite difference and finite element methods agree well with each other.